Received: 9 December 2020 | Revised: 1 March 2021 | Accepted: 23 March 2021

DOI: 10.1002/rcm.9094

RESEARCH ARTICLE

Rapid Communications in Mass Spectrometry WILEY

Improved plasma stoichiometry recorded by laser ablation ionization mass spectrometry using a double-pulse femtosecond laser ablation ion source

Andreas Riedo | Rustam Lukmanov | Valentine Grimaudo | Coenraad de Koning | Niels F. W. Ligterink | Marek Tulej | Peter Wurz

Physics Institute, Space Research and Planetary Sciences, University of Bern, Sidlerstrasse 5, Bern, 3012, Switzerland

Correspondence
A. Riedo, Physics Institute, Space Research and Planetary Sciences, University of Bern, Sidlerstrasse 5, 3012 Bern, Switzerland.
Email: andreas.riedo@space.unibe.ch

Funding information
Swiss National Science Foundation; Swiss National Science Foundation, Grant/Award Number: 193453

Rationale: Femtosecond (fs) laser ablation ion sources have allowed for improved measurement capabilities and figures of merit of laser ablation based spectroscopic and mass spectrometric measurement techniques. However, in comparison to longer pulse laser systems, the ablation plume from fs lasers is observed to be colder, which favors the formation of polyatomic species. Such species can limit the analytical capabilities of a system due to isobaric interferences. In this contribution, a double-pulse femtosecond (DP-fs) laser ablation ion source is coupled to our miniature Laser Ablation Ionization Mass Spectrometry (LIMS) system and its impact on the recorded stoichiometry of the generated plasma is analyzed in detail.

Methods: A DP-fs laser ablation ion source (temporal delays of +300 to − 300 ps between pulses) is connected to our miniature LIMS system. The first pulse is used for material removal from the sample surface and the second for post-ionization of the ablation plume. To characterize the performance, parametric double- and single-pulse studies (temporal delays, variation of the pulse energy, voltage applied on detector system) were conducted on three different NIST SRM alloy samples (SRM 661, 664 and 665).

Results: At optimal instrument settings for both the double-pulse laser ablation ion source and the detector voltage, relative sensitivity coefficients were observed to be closer (factor of ∼2) to 1 compared with single-pulse measurements. Furthermore, the optimized settings worked for all three samples, meaning no further optimization was necessary when changing to another alloy sample material during this study.

Conclusions: The application of a double-pulse femtosecond laser ablation ion source resulted in the recording of improved stoichiometry of the generated plasma using our LIMS measurement technique. This is of great importance for the quantitative chemical analysis of more complex solid materials, e.g., geological samples or metal alloys, especially when aiming for standard-free quantification procedures for the determination of the chemical composition.

1 | INTRODUCTION

Sensitive measurement techniques using a pulsed laser to probe the chemical composition of solids, e.g. Laser Ablation Inductively Coupled Plasma Mass Spectrometry (LA-ICP-MS), Laser-Induced Breakdown Spectroscopy (LIBS), or Laser Ablation Ionization Mass Spectrometry (LIMS), are applied in various fields in academic and industrial research to quantitatively investigate the chemical composition of solid samples. Applications range from, e.g., chemical imaging of highly heterogeneous geological and/or biological samples,[1–9] to the dating of solids and mineralogical analysis,[10,11] and to the chemical analysis of high-performance materials used in industry.[12–16] LA-ICP-MS is among the most widespread laser-based analytical technique due to its accurate quantification, high reproducibility, and low limits of detection. Today, various hybrid systems commercially exist that integrate both LA-ICP-MS and LIBS instrumentation to extend the measurement capabilities for the chemical analysis of solids.[17–20]

The application of a pulsed laser system to probe the analyte of interest has many advantages, as structures down to tens of nanometers can be targeted, layered materials can be chemically profiled by consecutive laser pulses, and sample contamination via handling can be minimized as no mechanical or chemical contact is required during preparation, among others.[9,21,22] With the replacement of, e.g., nanosecond or picosecond laser systems with powerful and stable ultra-fast pulsed femtosecond laser systems, the analytical capabilities and figures of merit of all laser-based measurement techniques have improved significantly, including, e.g., minimized matrix effects and element fractionation effects due to the absence of laser plasma plume interaction, improvement of spatial resolution due to reduced heat dissipation, increased reproducibility of measurements, enhanced ionization and stoichiometry, among others.[23–27] The application of femtosecond laser systems, however, shows drawbacks as well, at least for LIMS and LIBS systems. The resulting ablation plasma produced by such systems is colder and the lifetime is shorter than those induced by longer pulsed laser systems.[28] The colder plasma temperature favors the formation of polyatomic species in the ablation plume[28] and, depending on the analytical tool used for chemical quantification, the analytical capabilities may be limited if the mass resolving power is not high enough to discriminate against these isobaric interferences. For LIBS, the shorter lifetime of the plasma decreases the signal-to-noise ratio of detected signals and therefore limits the detection sensitivity.[29]

In this contribution, we quantify the analytical performance of a collinear double-pulse (DP) femtosecond (fs) laser ablation ion source that is coupled with our LIMS system.[30] The measurement will show that, at optimal instrument settings, in particular of the DP laser ablation/ionization source and the detector, the relative sensitivity coefficients (RSC), required for quantification of the chemical composition of solids, can be improved significantly; they scatter closer to 1. The application of a DP-fs laser ion source was introduced previously in LIBS and LA-ICP-MS instrumentation (see, e.g.,[29,31–34]). In LIBS, post-heating of the plasma by a second laser pulse allows for, e.g., a longer-lived plasma and, as a result, improved detection limits. In LA-ICP-MS, the DP measurement scheme allowed, e.g., for the generation of a more fine-grained aerosol, which is highly favorable for the ICP. Recently, we demonstrated by studies on a Mg sample that the application of the DP mode allowed an increase in ion yield relative to the single-pulse (SP) mode by a factor of up to about 30.[30] In the current study, we apply longer than typically applied delays between the two laser pulses and analyze monoatomic ions produced in such a configuration. To the best of our knowledge, this is the first contribution reporting about the impact of a DP-fs system on the quantitative performance of a LIMS system with the second pulse used for post-ionization of atoms.

2 | EXPERIMENTAL

2.1 | Sample materials

For performance characterization, measurements on three different National Institute of Standards and Technology (NIST) standard reference material (SRM) alloys were conducted: SRM 661, 664, and 665. Prior to measurements, the top surface was removed mechanically with a diamond file and cleaned using an argon ion sputter gun (ion energy of about 3 keV, a 10 degree incident angle, and sputtering time of about 20 min).[23] The samples were selected for this study because many previous studies were conducted on these samples using our miniature LIMS system to which different laser systems were connected, from nanosecond[35,36] laser systems (operated at IR and UV wavelengths) to femtosecond laser systems.[23]

2.2 | Laser ablation ionization mass spectrometer

The measurement capabilities and principles of operation of the mass spectrometric system used for the performance characterization of the DP ablation ion source are described in detail in various scientific contributions.[3,23,36–38] Therefore, only a brief description of the measurement principles of the system, based on SP laser ablation, is given in the following.

The system used for recording mass spectra is a miniature (mass analyzer with 160 × Ø 60 mm) reflectron-type time-of-flight (TOF) mass spectrometer that was originally designed for the *in situ* analysis of the chemical composition of solids on planetary surfaces. The mass spectrometer is located within a vacuum chamber and a beam guiding system is used to guide the laser pulses towards the entrance window of the chamber. The laser pulses are focused by an optical lens system positioned directly above the mass analyzer, through the system, and towards the sample surface, which is positioned roughly 1 mm below the entrance ion optics of the mass spectrometer. In the current design, only positively charged species can enter the ion optical system. At the entrance of the system the ions are accelerated, focused, and confined into the field-free drift path of the mass analyzer. At the ion mirror, the ions are reflected towards the

multichannel (MCP) detector system[37] by passing the field-free drift path for a second time. The ions are separated in the field-free drift paths according to their mass-to-charge ratio, following the TOF measurement principle. The quadratic equation $m(t) = k_0(t - t_0)^2$ is used for the conversion of a TOF to a mass spectrum, where k_0 and t_0 are fitting constants. Note that the mass resolving power of this miniature mass analyzer allows for discrimination of different isotopes, but is not sufficient to resolve isobaric interferences, e.g., doubly charged ^{56}Fe cannot be distinguished from singly charged ^{28}Si. In this study, only two out of four anodes of the MCP detector system were used for the characterization of the DP ion source. A high negative voltage at the front, and a less negative voltage at the back of the MCP stack (chevron configuration), are applied to guide the released electrons towards the anodes. The back voltage was kept during the measurements at −300 V, while the front was varied in the measurements. The applied detector voltage mentioned in the following refers to the high negative one. Two high-speed ADC cards (each with two channels, channels were combined on each card resulting in a doubled sampling rate of 3.2 GS/s, 12-bit vertical resolution, with onboard processing capabilities) were used for the recording of TOF spectra. For characterization of the recorded mass spectra, in-house written software is used, which allows for, e.g., TOF to mass scale conversion, peak integration, and the calculation of RSC values.[39] In this study, we consider certified elements in the SRM samples until Fe for calculation of RSC values. Iron is the most abundant species in these samples and gain-loss was observed which affects the derived RSC values. Similar to our earlier studies, the RSC value of a certain element is calculated via measured abundance divided by the NIST certified abundance. The samples are positioned below the mass spectrometer using a three-dimensional (3D) micro-translation stage with micrometer positioning accuracy. The complete instrument setup, including laser system, acquisition card, sample stage and delay stage (discussed in the following), are fully controlled remotely by in-house written software.

The fs laser system used in this study is operated at a wavelength of $\lambda = 775$ nm and a laser pulse repetition rate of 1 kHz, and produces pulse widths of $\tau \sim 190$ fs. The mechanical realization of the collinear DP system was described in detail in Tulej et al,[30] and is described only briefly in the following. The fundamental laser beam (p-polarization) is first transformed to an s-polarized beam via a half-wave plate (denoted as WP in Figure 1) installed directly at the output of the laser system before being split into two beams. An s-polarization sensitive 50/50 beam splitter (denoted as BS1) was used for beam splitting. The pulses from one beam are guided to a static beam guiding system (defined as P1) that is composed of a static retroreflector system and a polarization-sensitive attenuator (denoted as A). In comparison to the first realization of the DP system described in Tulej et al,[30] this static retroreflector was added to the beam guiding system because it enables correction for small deviations between the travelling paths between both laser beams. Further, it allows the same beam characteristics, such as the polarization of both beams. It is known that the integration of retroreflector systems affects the polarization of the incoming beam;

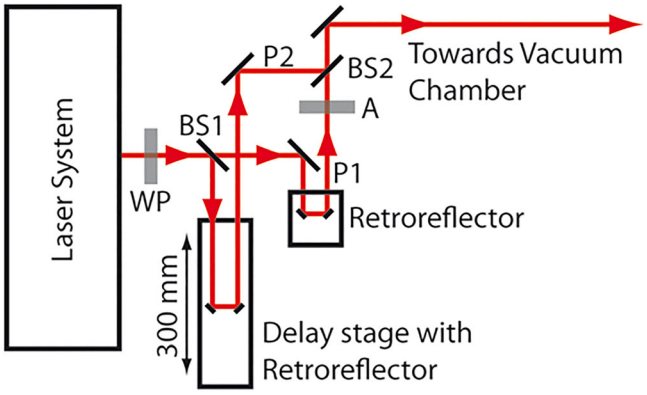

FIGURE 1 Schematics of the collinear DP-fs laser ablation ion source. The integrated retroreflector positioned on a remotely controlled linear stage allows for variation of the delay between both laser pulses with delay increments of ∼300 fs. Further information is given in the text

see, e.g., the technical note from Thorlabs regarding the integration of a prism retroreflector or theoretical calculations.[40,41] Pulses from the second beam are guided to a dynamic beam guiding system (denoted as P2). The latter system is composed of a retroreflector that is positioned on a remotely controlled linear stage with a traveling distance of 300 mm. The dynamic guiding system is installed in such way that delays relative to P1 of +300 to −300 ps can be realized with time increments of ∼300 fs. The energy of both laser pulses can be changed by either adjusting the output power of the main laser system or using the attenuator installed in the static beam guiding system. A second beam splitter (BS2) is used finally to recombine the beams of both beam-guiding systems. From that position, both pulses follow the same beam path towards the mass spectrometer.

2.3 | Measurement procedure

For the quantification of the effect of the DP ion source on the analytical performance of the system, multi-parametric studies are required (e.g., applied pulse energy, the delay between P1 and P2, etc.). First, a laser irradiance campaign (16 different pulse energies in the range of ∼400 nJ to 7.48 μJ were applied) in SP mode was conducted on SRM 664. Each measurement of different pulse energy was performed on a new and unused sample position. A total of 100,000 laser shots were applied on each sample position for each pulse energy, resulting in 100,000 spectra, which were stored on the host computer in packages of 1000 histogrammed spectra, resulting in 100 saved TOF spectra. This campaign allowed to define, e.g., the laser ablation threshold, the maximum pulse energy before observing space charge effects, and, most importantly, the pulse energy conditions where stable ablation can be observed. Note that SP measurements were conducted using the static beam guiding system (P1, see Figure 1) because of the integrated beam attenuator that allows easy adjustments of the laser pulse energy. Subsequently,

dense raster campaigns were applied on NIST 664 to investigate the impact of the delay between P1 and P2 on the plasma stoichiometry. The raster campaign consisted of 2000 sample positions with a pitch of 30 μm and was repeated for three different pulse energies (1.8 μJ, 2.1 μJ, and 2.7 μJ) with both pulses set at the same energy. Each sample position in the raster campaign involved a different delay between P1 and P2 with a delay increment of ∼300 fs. For each delay, four files of 4000 spectra were recorded and saved on the host computer. These raster campaigns were required to define, e.g., the zero delay between both pulses from P1 and P2, the delay where the hottest plasma conditions can be observed (reduction of polyatomic species), or the regime where mostly post-ionization of the generated plasma occurs. With the knowledge of these regimes, measurement campaigns conducted with the single- and double-pulse scheme (where the total applied pulse energy in both campaigns was the same) were conducted on fresh and unused sample positions. At optimal measurement conditions (laser and detector settings), DP measurements were finally extended to SRM 661 and 665 to assess the broader applicability of the found measurement parameters.

3 | RESULTS AND DISCUSSION

Through the SP laser irradiance campaign, the laser ablation threshold (close to 1 μJ), as well as the regime where a stable ablation is obtained, was identified. Stable and continuous ablation occurred at about 1.8 μJ, whereas at lower pulse energies, only major abundant elements were identified in the recorded and histogrammed spectra (data not shown). The information of, e.g., the ablation threshold is of importance for the application of the DP ion source. DP studies near but above the ablation threshold energy (considering first laser pulse applied) have several advantages, including, e.g., reduced surface and space charge effects. These effects impact the spectral quality; peak distortion and spectral jitter are reduced, which in turn improves the mass resolution. Moreover, for sufficiently low plasma densities, less laser radiation shielding effects occur and the second laser pulse can penetrate through the plasma plume more efficiently.

In Figure 2, the recorded signals (integrated peak intensity) of $^{56}Fe^{+}$ (right panels) and $^{56}Fe_2^{+}$ (left panels) of two delay campaigns conducted at a total applied pulse energy of 2.1 μJ and 2.7 μJ are presented (the detector was operated at voltages of −1850 V and −1900 V for the 2.7 μJ and 2.1 μJ campaign, respectively). Note that each data point corresponds to the mean of the recorded signal of the four histogrammed TOF spectra (each file is a histogram of 4000 spectra). A moving average filter (window size of three data points) was applied for better visualization of the recorded data. Iron is the major abundant element of NIST 664 and, hence, the positively charged dimer $^{56}Fe_2^{+}$ can be formed and observed readily in the plume. The delay campaigns show three different regimes; R1 where a zero delay between both pules is achieved, R2 where conditions with the hottest plasma are reached, and R3 where mostly post-ionization takes place (see notations in the top left panel). A similar signal trend was reported in an earlier publication where measurements were conducted in DP mode on a Mg sample.[30] At a zero delay (indicated with a dashed line), which is virtually identical to the situation where one single laser pulse with double energy is applied (see discussion below for Figure 3), a small signal enhancement can be identified (see insert in the bottom left panel). Note that the raster campaigns were conducted with a delay accuracy of ∼300 fs for the identification of the zero delay. A slight imperfection at zero delay between both laser pulses may result in a slightly reduced signal due to potential interference effects. Right and left from this localized signal enhancement a smooth drop is recognizable, which is then followed by a large increase in the signal,

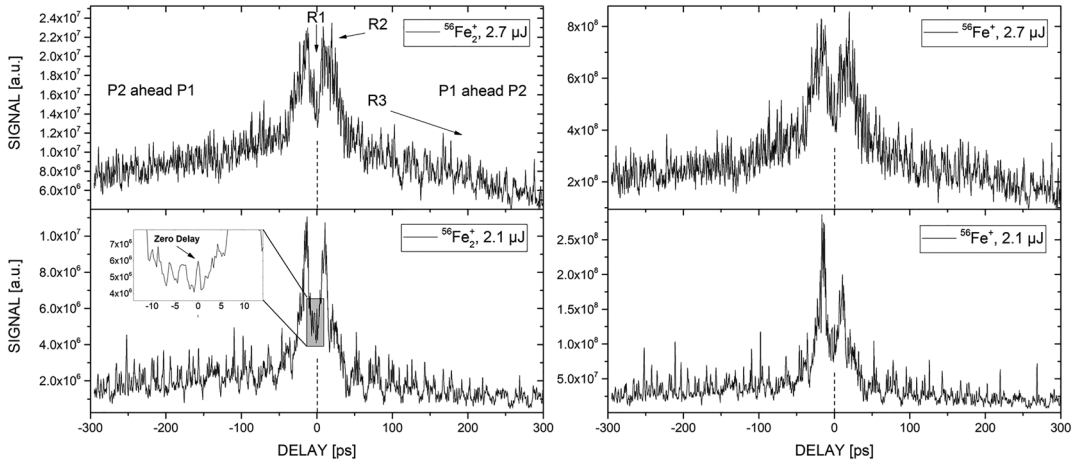

FIGURE 2 Two pulse delay campaigns conducted at two different total pulse energies are shown (2.1 μJ and 2.7 μJ). The time shift between both pulses was probed between −300 and +300 ps. In total, 2000 delays were investigated, with a delay increase of ∼300 fs between each step. For both campaigns, the recorded signal of $^{56}Fe_2^{+}$ (left panels) and of $^{56}Fe^{+}$ (right panels) are plotted. Three regimes can be identified (see top left panel), with R1 corresponding to the regime of zero delay, R2 to the hottest plasma condition, and R3 to the regime where mostly post-ionization of the neutral atoms in the ablated plume takes place

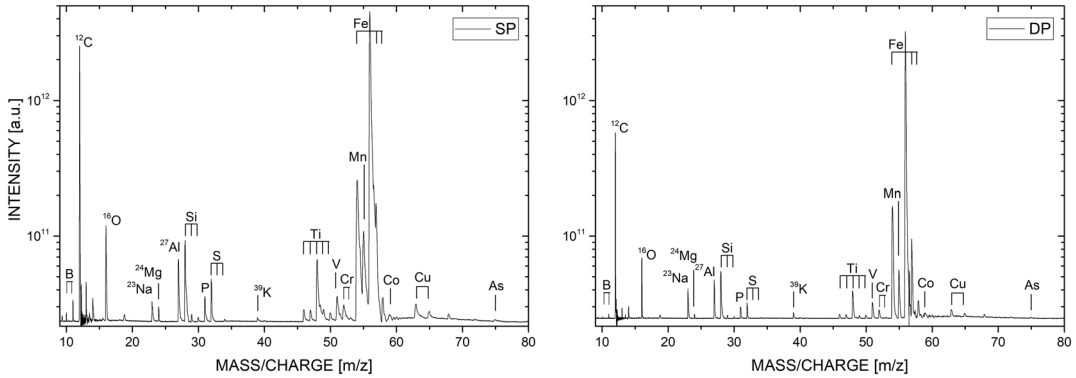

FIGURE 3 Mass spectra of NIST 664 recorded in SP mode (left) and DP mode (right), both recorded at the same total applied pulse energy of 3.5 μJ. The delay in the DP mode was zero (R1 regime in Figure 2). In comparison to the SP measurement, slightly lower intensities are observed for the DP measurement. Note that the scaling of both panels is identical

forming the regime of hottest plasma conditions at a delay of about 25 ps, comparable with our previous study conducted on a Mg sample.[30] At these conditions, neutral species that are produced during the ablation process are efficiently post-ionized, resulting in a significant increase in the overall recorded signal. Note that the increase in recorded signal for atomic species is higher than the production of, e.g., positively charged dimers at hottest plasma conditions, leading to a net reduction in such species contribution, as also determined by Tulej et al.[30,42] For the measurement conducted at a pulse energy of 2.7 μJ (see Figure 2), a net gain of positively charged ^{56}Fe relative to the dimer $^{56}Fe_2$ of ~10% was observed. Note that the effect of DP post-ionization is more efficient at lower applied pulse energies. This effect is expected because the post-ionization is more efficient having a lower density plasma produced.[30] Note that, before starting these delay campaigns, special attention was given to achieve equal pulse energy and comparable ablation profiles for both pulses. This explains why the signal evolution in Figure 2 is almost symmetrical around zero delay. After passing the hot plasma conditions, a steep drop in recorded signal is observed, which is comparable with our earlier study conducted on a Mg sample (see Tulej et al, fig. 4).[30]

For verification, i.e., if the DP mode with zero delay between the two pulses produces a comparable signal to SP mode, three measurements of both modes working at the same total energy of 3.5 μJ and detector voltage of −1850 V were conducted (see Figure 3). Note that, for this study, as shown in Figure 3, the pulse energy of 3.5 μJ was selected, because from SP measurements it is known that a pulse energy of 3.5 μJ allowed for stable and continuous material ablation (ablation threshold was observed at ~1 μJ). The shown measurements are an accumulation of 100,000 single mass spectra (100 files, each corresponding to a histogrammed spectrum of 1000 single spectra). Note that the y-axis scaling is identical for both panels and that the recorded signal is displayed in log-scale. In comparison to the SP measurements, a slightly lower recorded signal can be observed for the DP measurements at zero delay. This effect can be attributed to the accuracy of ~300 fs for the identification of the zero delay between both laser pulses. As discussed in the previous paragraph, a slightly imperfect overlap between both pulses results immediately in a reduced signal. Interestingly, small differences between the conducted SP and DP ablation measurements were observed. In comparison to the SP measurements, in all three measurements conducted in DP mode lower intensities for Ti and S were observed. The SP measurements are in line with previous measurements; typically, a much higher ion yield of Ti relative to other monoatomic ions was observed. In the study of Neuland et al,[43] measurements were conducted on four geological standard materials and Ti showed consistently an elevated RSC value at the level of about 10 (fig. 5 in Neuland et al[43]). In the DP measurement, the measured signal of Ti is lower, which is closer to the actual stoichiometry of the ablated material. Interference effects in close vicinity of a perfect zero delay might be a possible source for this observation – the electrons can be heated for a slightly longer time which might improve the ionization of the ablated material. In addition to this observation, a better resolved mass spectrum is observed for the DP measurement, which may be accounted to, e.g., reduced surface charge effects. This observation cannot be generalized for all DP measurements. For instance the DP measurement displayed and discussed in the following Figure 4 shows a comparable mass resolution to the SP measurement (see mass-to-charge region of the Fe isotopes). Note that the ion optical system of the employed TOF mass spectrometer can typically handle low intensity plasmas better than high intensity ones.

A similar observation of reduced ion yield of Ti was found in DP measurements conducted at hottest plasma conditions (see regime R2 in Figure 2). The left panel of Figure 4 shows a section of the simulated mass spectrum of NIST 664 around Ti, whereas, in the middle and right panels, the actual SP and DP measurements are shown. Again, both the SP and DP measurement campaigns were conducted at almost identical measurement settings. The applied pulse energy was ~3.4 μJ and ~3.5 μJ for the DP and SP measurement campaign, respectively. Both measurements were performed with the same detector voltage of −1850 V. The shown parts of the SP and DP spectra correspond to histogrammed spectra of 30,000 spectra each. All three spectra are normalized to $^{54}Fe^+$. The

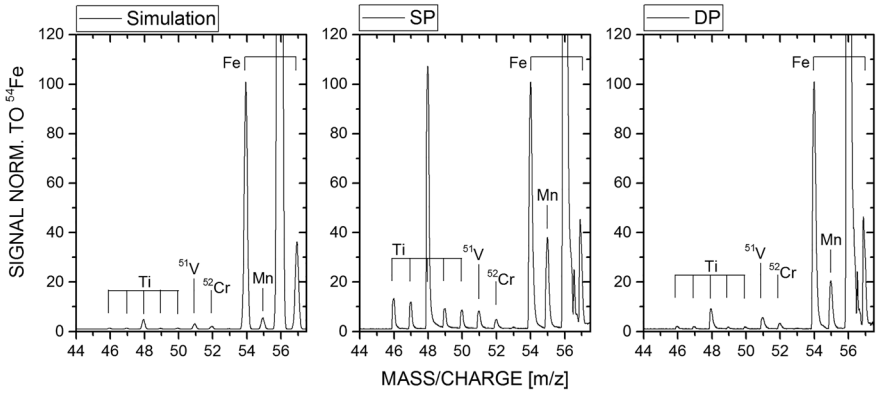

FIGURE 4 Left: Simulated mass spectrum of NIST 664 around Ti; middle: single-pulse (SP) measurement; right: DP measurement at hottest plasma conditions (R2, see Figure 2). For comparison, the simulated and recorded signals were normalized to $^{54}Fe^{+}$. The total applied pulse energy was almost identical in the SP (~3.5 μJ) and DP (~3.4 μJ) measurement mode

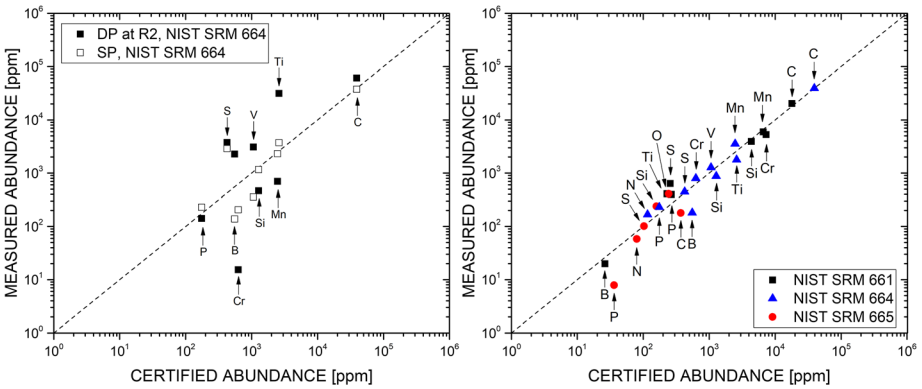

FIGURE 5 Left: RSC values calculated for the case of DP measurements at hottest plasma conditions (R2) and SP measurements at the same total pulse energy. Right: RSC values derived for best instrument settings in the DP mode, i.e., pulse energy, pulse delay, and detector gain. In comparison with the RSC values displayed on the left side, the RSC factors scatter much closer around 1 in a fully optimized system operated in DP mode at the optimal delay

simulated spectrum (all elements have RSC = 1) was generated using our in-house designed analysis software that provides the option to simulate spectra with, e.g., user-defined noise, observed mass resolution, or element/isotope abundances of a reference sample.[39] It can be clearly asserted that the Ti abundances recorded in the DP measurements match much better the known composition as shown in the simulated spectrum, while the relative recorded intensity of Ti in SP mode is significantly too high. This indicates that post-heating and post-ionization of the generated plasma with the second pulse improves the quantitative measurement at these specific instrument settings and pulse delay (hottest plasma condition).

Optimal measurement settings in view of element RSC could be derived by tuning (i) the delay of the second pulse in DP mode, (ii) total pulse energy, and (iii) applied detector voltage (an increase of ion signal, e.g., 30 times, can lead to ion detector saturation effects). Concerning the pulse delay, optimal measurement conditions were identified for measurements conducted in regime R3 (delay of ~300 ps), with a total applied pulse energy of ~ 5.8 μJ. Furthermore, the optimization included the reduction of the applied voltage at the MCP stack detector. A higher total applied voltage results in higher gain but also increases the probability to induce gain losses. Optimal detector settings were found at moderate amplification conditions to avoid such saturation effects and gain losses. A total potential difference of about 1450 V was applied over the MCP stack, which represents a compromise between signal amplification[37] and detector saturation and gain loss. Nevertheless, a sensitivity drop was observed at the arrival of ^{54}Fe ions, which is the second-highest abundant isotope of Fe, with iron being the most abundant element in all three investigated samples. To stay away from the detector limitations, we limited the analysis of RSC values for certified elements arriving earlier than ^{56}Fe, more precisely until ^{55}Mn.

In Figure 5, the RSC values of three different measurement conditions are shown. Note that all the measurements were conducted at the same detector voltage and applied total pulse energy of ~5.8 μJ. The left panel contains RSC values for NIST 664 derived from SP and DP measurements (R2, hottest plasma conditions). The right-hand panel presents the RSC values derived from the three NIST SRMs 661, 664, and 665 samples at the best instrument settings (delay ~300 ps, pulse energy of ~5.8 μJ, and applied detector voltage of ~ −1750 V). Note that the detector voltage and the total applied pulse energy were kept the same for the individual measurements inside the same panel.

The RSC values for SP measurements (Figure 5, left panel) scatter around the trend line of 1 (dashed line), which is comparable to previous measurements. Surprisingly, the RSC values for the DP measurements conducted at the hottest plasma regime scatter slightly more than the SP measurements. A possible explanation could be that the produced number of ions cannot be accounted for correctly by the ion optical and detector system of our miniature LIMS system. The situation is very different for measurements conducted at optimal conditions (pulse delay and energy, and detector voltage). As can be observed in the right panel of Figure 5, the scatter of the RSC values is much less, values are closer to 1. Note that Al was not considered for calculation of RSC values because of potential isobaric interferences with doubly charged ^{54}Fe. Note that for measurements conducted on SRM 665, the RSC values of N and O are shown as well

and match very well with the trend line representing RSC = 1. These are the only two elements shown for which NIST provides a non-certified estimate abundance based on a single instrument technique, rather than a certified abundance as for all other shown elements. In addition to the graphical representation of the RSC values derived for the measurements show in Figure 5, the improvement can be quantified using the following two equations:

$$a = \frac{1}{n}\sum_{i}^{n} |\log(\mathrm{RSC}_i)|; \text{ and } b = (1-a) * 100;$$

where RSC_i denotes the RSC value of element i and n the number of RSC values available for the quantification. The absolute value of the logarithmic value of the RSC is required because in this way both RSC values of 0.1 and 10 have the same weight for the quantification of the sum (both are a factor of 10 off). The closer a is to 0, and b is to 100, the better the quantification of the elements by the applied instrument setting. Note that for this calculation, only the RSC values derived for SRM 664 are considered (SP measurement, DP measurement conducted in hottest plasma conditions, and DP at optimal conditions, see Figure 5). For the SP measurement, we derive for $a = 0.31$ and $b = 69$, for the DP hottest plasma conditions $a = 0.67$, $b = 33$, and for DP at optimal conditions $a = 0.14$ and $b = 86$. This quantification shows that the DP measurements conducted at optimal conditions are by a factor of about 2 closer to the optimal situation (14% off for DP measurements at best settings, and 31% for the SP measurements). As mentioned before from visual inspection of Figure 5, the quantification shows as well that the DP measurements conducted at hottest plasma conditions were less optimal than the SP measurements. Tulej et al[30] showed that the post-ionization at hot plasma conditions is very effective. However, in this study, such conditions might lead to a too dense plasma of positively charged species, which may exceed the capabilities of the ion optical system of our miniature TOF-MS system, which in turn would lead to limited resolution in the TOF spectrum, limiting the accuracy of, e.g., peak integration.

At the optimal conditions, lower signal intensity was typically observed as well, which may reduce the detection sensitivity of the applied instrument. However, such conditions may still be of high importance when a matrix-matched standard is not available for the analysis of an unknown sample. Important to note is that the larger RSC scatter (e.g., left panel of Figure 5) is not a limiting factor for the mass spectrometric quantification of solids using LIMS. In case a matrix-matched standard is available, the RSC values derived from the standard can be applied to an unknown sample, even if the applied measurement conditions lead to a larger variation in RSC values between different elements.

4 | CONCLUSIONS

Previous studies have shown that the coupling of femtosecond (fs) laser systems to the LIMS technique allows for the improvement of various figures of merits, ranging from clean and reliable chemical depth profiling to improved stoichiometry of the generated plasma. In this contribution, we demonstrate that the application of a DP-fs laser ablation ion source leads to an improved stoichiometry of the generated plasma. The second laser pulse supports the ionization of the atoms generated during the ablation as a result of the first pulse, which overall improves the stoichiometry of the recorded plasma. The optimization of both laser settings (delay and pulse energy) and detector system allowed the identification of the most suitable measurement conditions. Calibration factors, RSC values, for the investigated NIST steel alloys SRM 661, 664, and 665 are observed to be close to 1, which is of interest to measurement campaigns on unknown samples where the availability of matrix-matched reference samples is limited.

ACKNOWLEDGEMENTS

This work is supported by the Swiss National Science Foundation. NFWL is supported by the Swiss National Science Foundation Ambizione grant No. 193453.

DATA AVAILABILITY STATEMENT

The data that support the findings of this study are available from the corresponding author upon reasonable request.

ORCID

Andreas Riedo https://orcid.org/0000-0001-9007-5791
Rustam Lukmanov https://orcid.org/0000-0001-9257-7410
Valentine Grimaudo https://orcid.org/0000-0002-7010-5903
Coenraad de Koning https://orcid.org/0000-0002-2540-7689
Niels F. W. Ligterink https://orcid.org/0000-0002-8385-9149
Marek Tulej https://orcid.org/0000-0001-9823-6510
Peter Wurz https://orcid.org/0000-0002-2603-1169

REFERENCES

1. Neubeck A, Tulej M, Ivarsson M, et al. Mineralogical determination in situ of a highly heterogeneous material using a miniaturized laser ablation mass spectrometer with high spatial resolution. *Int J Astrobiol*. 2015;15:133-146.
2. Tulej M, Neubeck A, Ivarsson M, et al. Chemical composition of micrometer-sized filaments in an aragonite host by a miniature laser ablation/ionization mass spectrometer. *Astrobiology*. 2015;15(8):669-682.
3. Wiesendanger R, Wacey D, Tulej M, et al. Chemical and optical identification of micrometer-sized 1.9 billion-year-old fossils by combining a miniature laser ablation ionization mass spectrometry system with an optical microscope. *Astrobiology*. 2018;18:1071-1080.
4. Yan W, Casey JF. A new concordia age for the 'forearc' bay of islands ophiolite complex, Western Newfoundland utilizing spatially-resolved LA-ICP-MS U-Pb analyses of zircon. *Gondw Res*. 2020;86:1-22.
5. Chen G, Gao J, Lu J, Zhang R. In situ LA-ICP-MS analyses of mica and wolframite from the Maoping tungsten deposit, southern Jiangxi, China. *Acta Geochim*. 2020;39(6):811-829.
6. Ye Y, Wang H, Wang X, Zhai L, Wu C, Zhang S. Elemental geochemistry of lower Cambrian phosphate nodules in Guizhou Province, South China: An integrated study by LA-ICP-MS mapping and solution ICP-MS. *Palaeogeogr Palaeoclimatol Palaeoecol*. 2020;538:109459.
7. Grijalba N, Legrand A, Holler V, Bouvier-Capely C. A novel calibration strategy based on internal standard–spiked gelatine for quantitative bio-imaging by LA-ICP-MS: Application to renal localization and quantification of uranium. *Anal Bioanal Chem*. 2020;412(13):3113-3122.

8. Vogt DS, Schröder S, Rammelkamp K, Hansen PB, Kubitza S, Hübers HW. CaCl and CaF emission in LIBS under simulated Martian conditions. *Icarus*. 2020;335:113393.
9. Green T, Kuznetsov I, Willingham D, et al. Characterization of extreme ultraviolet laser ablation mass spectrometry for actinide trace analysis and nanoscale isotopic imaging. *J Anal At Spectrom*. 2017;32(6):1092-1100.
10. Liu Y, Hu Z, Gao S, et al. In situ analysis of major and trace elements of anhydrous minerals by LA-ICP-MS without applying an internal standard. *Chem Geol*. 2008;257(1-2):34-43.
11. Chang Z, Vervoort JD, McClelland WC, Knaack C. U-Pb dating of zircon by LA-ICP-MS. *Geochem Geophys Geosyst*. 2006;7(5):1-14.
12. Moreno-García P, Grimaudo V, Riedo A, et al. Towards structural analysis of polymeric contaminants in electrodeposited cu films. *Electrochim Acta*. 2016;199:394-402.
13. Moreno-García P, Grimaudo V, Riedo A, Tulej M, Wurz P, Broekmann P. Towards matrix-free femtosecond-laser desorption mass spectrometry for in situ space research. *Rapid Commun Mass Spectrom*. 2016;30(8):1031-1036.
14. Lee S, Gonzalez JJ, Yoo JH, Chirinos JR, Russo RE, Jeong S. Application of femtosecond laser ablation inductively coupled plasma mass spectrometry for quantitative analysis of thin Cu(In,Ga)Se_2 solar cell films. *Thin Solid Films*. 2015;577:82-87.
15. Hou H, Cheng L, Richardson T, et al. Three-dimensional elemental imaging of Li-ion solid-state electrolytes using fs-laser induced breakdown spectroscopy (LIBS). *J Anal At Spectrom*. 2015;30(11):2295-2302.
16. Gutierrez-Gonzalez A, Gonzalez-Gago C, Pisonero J, et al. Capabilities and limitations of LA-ICP-MS for depth resolved analysis of CdTe photovoltaic devices. *J Anal At Spectrom*. 2015;30(1):191-197.
17. Dong M, Wei L, González JJ, et al. Coal discrimination analysis using tandem laser-induced breakdown spectroscopy and laser ablation inductively coupled plasma time-of-flight mass spectrometry. *Anal Chem*. 2020;92(10):7003-7010.
18. Syta O, Wagner B, Bulska E, et al. Elemental imaging of heterogeneous inorganic archaeological samples by means of simultaneous laser induced breakdown spectroscopy and laser ablation inductively coupled plasma mass spectrometry measurements. *Talanta*. 2018;179:784-791.
19. Bonta M, Gonzalez JJ, Quarles CD, Russo RE, Hegedus B, Limbeck A. Elemental mapping of biological samples by the combined use of LIBS and LA-ICP-MS. *J Anal At Spectrom*. 2016;31(1):252-258.
20. Bonta M, Limbeck A. Metal analysis in polymers using tandem LA-ICP-MS/LIBS: Eliminating matrix effects using multivariate calibration. *J Anal At Spectrom*. 2018;33(10):1631-1637.
21. Grimaudo V, Tulej M, Riedo A, et al. UV post-ionization laser ablation ionization mass spectrometry for improved nm-depth profiling resolution on Cr/Ni reference standard. *Rapid Commun Mass Spectrom*. 2020;34:e8803.
22. Käser D, Hendriks L, Koch J, Günther D. Depth profile analyses with sub 100-nm depth resolution of a metal thin film by femtosecond - laser ablation - inductively coupled plasma - time-of-flight mass spectrometry. *Spectrochim Acta Part B: At Spectrosc*. 2018;149:176-183.
23. Riedo A, Neuland M, Meyer S, Tulej M, Wurz P. Coupling of LMS with a fs-laser ablation ion source: Elemental and isotope composition measurements. *J Anal At Spectrom*. 2013;28(8):1256.
24. Zhang B, He M, Hang W, Huang B. Minimizing matrix effect by femtosecond laser ablation and ionization in elemental determination. *Anal Chem*. 2013;85(9):4507-4511.
25. Hergenröder R, Samek O, Hommes V. Femtosecond laser ablation elemental mass spectrometry. *Mass Spectrom Rev*. 2006;25(4):551-572.
26. Russo RE, Mao X, Gonzalez JJ, Mao SS. Femtosecond laser ablation ICP-MS. *J Anal At Spectrom*. 2002;17(9):1072-1075.
27. Zeng X, Mao XL, Greif R, Russo RE. Experimental investigation of ablation efficiency and plasma expansion during femtosecond and nanosecond laser ablation of silicon. *Appl Phys A*. 2005;80(2):237-241.
28. Hou H, Mao X, Zorba V, Russo RE. Laser ablation molecular isotopic spectrometry for molecules formation chemistry in femtosecond-laser ablated plasmas. *Anal Chem*. 2017;89(14):7750-7757.
29. Labutin TA, Lednev VN, Ilyin AA, Popov AM. Femtosecond laser-induced breakdown spectroscopy. *J Anal At Spectrom*. 2016;31(1):90-118.
30. Tulej M, Wiesendanger R, Riedo A, Knopp G, Wurz P. Mass spectrometric analysis of the mg plasma produced by double-pulse femtosecond laser irradiation. *J Anal At Spectrom*. 2018;33(8):1292-1303.
31. Piñon V, Fotakis C, Nicolas G, Anglos D. Double pulse laser-induced breakdown spectroscopy with femtosecond laser pulses. *Spectrochim Acta Part B: At Spectrosc*. 2008;63(10):1006-1010.
32. Stratis DN, Eland KL, Angel SM. Dual-pulse LIBS using a pre-ablation spark for enhanced ablation and emission. *Appl Spectrosc*. 2000;54(9):1270-1274.
33. González J, Liu C, Yoo J, Mao X, Russo RE. Double-pulse laser ablation inductively coupled plasma mass spectrometry. *Spectrochim Acta Part B: At Spectrosc*. 2005;60(1):27-31.
34. Grassi R, Grifoni E, Gufoni S, et al. Three-dimensional compositional mapping using double-pulse micro-laser-induced breakdown spectroscopy technique. *Spectrochim Acta Part B: At Spectrosc*. 2017;127:1-6.
35. Tulej M, Iakovleva M, Leya I, Wurz P. A miniature mass analyser for in-situ elemental analysis of planetary material–performance studies. *Anal Bioanal Chem*. 2011;399(6):2185-2200.
36. Riedo A, Bieler A, Neuland M, Tulej M, Wurz P. Performance evaluation of a miniature laser ablation time-of-flight mass spectrometer designed for in situ investigations in planetary space research. *J Mass Spectrom*. 2013;48(1):1-15.
37. Riedo A, Tulej M, Rohner U, Wurz P. High-speed microstrip multi-anode multichannel plate detector system. *Rev Sci Instrum*. 2017;88(4):045114.
38. Grimaudo V, Moreno-García P, Riedo A, et al. High-resolution chemical depth profiling of solid material using a miniature laser ablation/ionization mass spectrometer. *Anal Chem*. 2015;87(4):2037-2041.
39. Meyer S, Riedo A, Neuland MB, Tulej M, Wurz P. Fully automatic and precise data analysis developed for time-of-flight mass spectrometry. *J Mass Spectrom*. 2017;52(9):580-590.
40. He W, Fu Y, Zheng Y, et al. Polarization properties of a corner-cube retroreflector with three-dimensional polarization ray-tracing calculus. *Appl Optics*. 2013;52(19):4527-4535.
41. Liu J, Azzam RMA. Polarization properties of corner-cube retroreflectors: Theory and experiment. *Appl Optics*. 1997;36(7):1553-1559.
42. Tulej M, Neubeck A, Riedo A, et al. Isotope abundance ratio measurements using femtosecond laser ablation ionization mass spectrometry. *J Mass Spectrom*. 2020;55(12):e4660.
43. Neuland MB, Grimaudo V, Mezger K, et al. Quantitative measurement of the chemical composition of geological standards with a miniature laser ablation/ionization mass spectrometer designed for in situ application in space research. *Meas Sci Technol*. 2016;27(3):035904.

How to cite this article: Riedo A, Lukmanov R, Grimaudo V, et al. Improved plasma stoichiometry recorded by laser ablation ionization mass spectrometry using a double-pulse femtosecond laser ablation ion source. *Rapid Commun Mass Spectrom*. 2021;35:e9094. https://doi.org/10.1002/rcm.9094